

Signatures of a Bardeen-Cooper-Schrieffer Polariton Laser

Jiaqi Hu¹, Zhaorong Wang², Seonghoon Kim², Hui Deng^{1,3*}, Sebastian Brodbeck⁴, Christian Schneider⁴, Sven Höfling^{4,5}, Nai H. Kwong⁶, Rolf Binder^{6,7*}

¹*Applied Physics Program, University of Michigan, Ann Arbor, MI 48109, USA*

²*Department of Electrical Engineering, University of Michigan, Ann Arbor, MI 48109, USA*

³*Department of Physics, University of Michigan, Ann Arbor, MI 48109, USA*

⁴*Technische Physik, Universität Würzburg, Am Hubland, Würzburg 97074, Germany*

⁵*SUPA, School of Physics and Astronomy, University of St Andrews, St Andrews KY16 9SS, United Kingdom*

⁶*College of Optical Sciences, University of Arizona, Tucson, AZ 85721, USA*

⁷*Department of Physics, University of Arizona, Tucson, AZ 85721, USA*

Microcavity exciton polariton systems can have a wide range of macroscopic quantum effects that may be turned into better photonic technologies^{1,2}. Polariton Bose-Einstein condensation (BEC) and photon lasing have been widely accepted in the limits of low and high carrier densities³, but identification of the expected Bardeen-Cooper-Schrieffer (BCS) state⁴ at intermediate densities remains elusive. While all three phases feature coherent photon emission, essential differences exist in their matter media. Most studies to date characterize only the photon field. Here, using a microcavity with strong- and weak-couplings co-existing in orthogonal linear polarizations, we directly measure the electronic gain in the matter media of

a polariton laser, demonstrating a BCS-like polariton laser above the Mott transition density. Theoretical analysis reproduces the absorption spectra and lasing frequency shifts, revealing an electron distribution function characteristic of a polariton BCS state but modified by incoherent pumping and dissipation.

Many material systems are well-known for exotic collective quantum effect. Ultracold atoms can exhibit BEC^{5,6}, conventional superconductors can exhibit the BCS state⁷, semiconductors in a resonant cavity can exhibit lasing⁸. Semiconductor microcavity polaritons, formed via strong coupling between bound electron-hole pairs and light, have been discussed to exhibit a range of many-body phases that bridge phenomena of both matter and light systems and involve both fermionic and bosonic quantum statistics^{4,9}. Three of the most studied phase transitions include the polariton BEC and polariton lasing transitions¹⁰ (Fig. 1b), the polaritonic BCS transition¹¹⁻¹³ (Fig. 1c), and the conventional lasing transition¹⁴ (Fig. 1d). As we compare in Fig. 1, while all three lead to coherent emission, they have distinct microscopic origins.

Exciton-polariton BEC takes place at carrier densities n much below the Mott transition density n_{Mott} , $n \ll n_{Mott}$, where electron-hole (e-h) pairs are bound by the Coulomb interaction to form excitons, which satisfy bosonic commutation properties (Fig. 1b)³. The electronic distribution functions are far below Fermi degeneracy and correspond to the exciton wavefunction. Coherence is formed via bosonic final state stimulation into the polariton ground state. Conventional photon lasing takes place in the limit of high densities $n \gg n_{Mott}$, where Coulomb interaction is screened, leading to uncorrelated, fermionic electron and hole plasmas. The electronic distribu-

tions are Fermi degenerate. Coherence is formed via stimulated scattering into a cavity mode when fermionic gain is provided by population inversion between the conduction and valence bands. In an intermediate regime, n is high enough to disallow stable, bound exciton states, but low enough to allow sufficient electron-hole Coulomb correlations. In this regime, absent a cavity, an excitonic BCS state, with a coherent population of degenerate and weakly Coulomb-bound e-h pairs, has been predicted since the 1960s¹⁵⁻¹⁸, though not yet demonstrated. In a strongly-coupled microcavity, different types of polariton BCS states have been proposed, with Coulomb or photon-induced electron-hole pairing^{4,12,13}.

Experimentally, emergence of a macroscopic quantum state via spontaneous symmetry breaking has been confirmed as the emitted light transforms from thermal to coherent¹⁹. Nonlinear interactions in the system have also been confirmed through the frequency shift²⁰ and coherence properties²¹ of the emitted light, which distinguishes a polariton laser from a photon laser. While the polariton laser has been commonly associated with an exciton-polariton BEC, its microscopic nature can not be directly identified from the light emission alone – both an exciton-polariton BEC and a BCS-like state would emit coherent light and show strong nonlinearities. The essential difference lies in the electronic media, which have been difficult to access experimentally.

In this work, we gain direct access to the electronic component in the presence of lasing, by using a cavity selective in linear polarizations. We measure both the absorption and emission spectra of both the electronic media and the lasing mode by combining off-resonant continuous wave pump with a resonant probe in time-resolved spectroscopy. Through this approach, we iden-

tify a polariton BCS state and show that, while it shares many spectral signatures nearly identical to those of a polariton BEC, it is unambiguously distinguished from a BEC by the fermionic nature of the gain as the mechanism for symmetry breaking. It is also distinguished from a photon laser as bound electronic states persist, manifested as an emission line that remains narrow, and an emission frequency that evolves continuously with pump density and remains much lower than the cavity resonance. To clarify the microscopic mechanism of the observed polariton laser, we develop a many-particle theory for the Coulomb correlated electron, hole and photon system. The theory correctly predicts the experimentally observed emission frequency and absorption spectra, and reveals distribution functions and inter-band polarizations resembling those of an ideal ($T=0K$) polariton BCS states^{12,13}, but modified by cavity dissipation and thermal dephasing.

To access the electronic media in the presence of polariton lasing, we use a cavity that simultaneously supports weakly- and strongly- coupled modes which, importantly, are in orthogonal linear polarizations. Schematics of our cavity system are shown in Fig. 1a. The top-mirror of the $\lambda/2$ cavity is made of a high-contrast sub-wavelength grating. The grating has very high reflectivity for transverse-electric (TE) polarized light, but low for transverse-magnetic (TM) polarized light (see Supplementary Information for the simulated reflectivity of the grating and electric field distribution in the cavity). As a result, TE polaritons are formed (Fig. 2a, Fig. S7) while TM excitons and photons remain in the weak-coupling regime (Supplemental Information Fig. S4, Fig. S5)²². In this configuration, we can access the reservoir (or bath) of the TE modes through the TM modes, as we explain below. Firstly, we use a linearly polarized non-resonant continuous-wave optical pump to supply a hot carrier population about 30 meV above the polariton resonance. These hot carriers

thermalize and form a reservoir for both TM and TE polaritons/excitons. This is confirmed by the observation of equal TE and TM emission outside the grating independent of the pump polarization (see Supplementary Information for the data and additional theoretical discussions). Secondly, the weakly- and strongly-coupled modes differ only over a small range of in-plane wavenumbers k_{\parallel} near $k_{\parallel} = 0$, where the TE ground state polariton density is estimated to be 10^{-4} of the total carrier density below threshold and $\sim 10^{-2}$ even at the highest power used. This ensures the TE and TM modes share essentially the same electron and hole reservoirs, despite very different dispersions and decay rates of the TE and TM modes near $k_{\parallel} = 0$. Hence, via polarization-resolved spectroscopy, we can access simultaneously the optical properties of the polariton system and its underlying electronic media.

We measure two distinct types of lasing transition for the TE-polarized modes in devices with different cavity-exciton detunings. In devices with negative to small positive detunings, polariton lasing was measured with features akin to a typical polariton BEC or polariton laser (top row in Fig. 2). In more blue-detuned devices, we observe clear features of a photon laser (bottom row in Fig. 2). We show an example of each in Fig. 2 and label them device I and II, respectively (see Supplementary Information for the corresponding TM spectra and animations of detailed evolution of the spectra with power for the polariton and photon lasers). Both device I and II show clean, discrete TE lower polariton modes at low excitation densities (Fig. 2a, left). At higher pumping densities, both devices reach a lasing transition, but they show distinct features in spectral linewidth and shift, one consistent with a polariton laser while the other a photon laser.

In device I, the ground state remains distinct throughout the measured densities, with only slight line-broadening below threshold and resolution-limited linewidth above threshold. Its frequency blue-shifts continuously with power and remains well below the cavity or exciton resonances (Fig. 2a,c, top). These features suggest the ground state remain as a coupled state between electron-hole pair and photon; they are the same as widely reported for polariton BECs in the literature^{19,23,24}.

In stark contrast, in device II, the lower polariton modes disappear as the pumping density increases (Fig. 2a, bottom middle panel, also see real-space spectra in Supplemental Information). A mode with a rather broad linewidth emerges near the cavity resonance frequency near the threshold and becomes pinned at the cavity frequency above threshold (Fig. 2c, bottom). These features are fully consistent with the dissociation of any bound state before transition to photon lasing. The result suggests that electron-hole plasma is formed in device II before it reaches a phase transition threshold. This may be because of both a heavier effective mass of the lower polaritons in device II that leads to a higher threshold density, and a larger exciton fraction that leads to stronger scattering-induced dephasing.

Similar photon lasing transitions in polariton cavities have also been studied in earlier works^{20,25,26}. Like in our observations, the photon lasing transitions were accompanied by significant linewidth broadening, many times more than that of a polariton lasing transition^{20,26}, as is consistent with the disappearance (retaining) of a bound state for photon (polariton) lasing transition. In some of these works, the photon lasing frequency was reported to be below the original cavity resonance when

the detuning is within about ± 10 meV, which was attributed to a red-shift of the cavity resonance at high carrier densities^{25,26}. However no quantitative models were given to explain such a shift; and the carrier densities are likely much higher than used in this study. The detuning of our device I and II are similar in magnitude, -2.4 meV and +3.5 meV, respectively; in device II, photon lasing takes place close to the original cavity resonance despite a higher threshold density than that of device I. This confirms that there is negligible shift of the cavity resonance in our devices at the carrier densities we used.

While devices like device I show spectral features distinct from a photon laser and similar to a polariton BEC, the absorption spectra of their electronic media reveal a many-body phase different from BEC. As described above, with linear polarization selectivity of the cavity, we are able to probe the electronic gain of the strongly coupled TE mode via the weakly coupled TM mode using time-resolved reflectance of a pulsed probe laser (see Methods for more details). As shown in Fig. 3a, without pump, we measure TM absorption at the exciton resonance below the band continuum and above the TE polariton energy. With increasing pump power but still below threshold, the exciton resonance disappears into the absorption edge of the band continuum. This implies that there is strong screening and band gap renormalization to lower energies, and that the carrier density is already near the Mott density. Close to threshold, a peak above unity emerges; its height and width increase with further increase of the pump power (Fig. 3a inset). This shows optical gain due to population inversion. Corresponding TE emission and reflection spectra are provided in the Supplementary Information.

We summarize in Fig. 3b the evolution of the resonances and gain with the pump power. The TM exciton resonance blue-shifts with increasing pump power but quickly broadens and becomes non-resolvable, corresponding to the Mott transition at moderate pump power well below threshold. In contrast, the discrete TE resonance continues to exist despite the Mott transition and the presence of gain in TM; it blue-shifts continuously with increasing carrier density throughout the pump powers used. Lasing takes place as the polariton ground state frequency enters the gain region and the frequency stays within the gain region at higher pump power, showing clearly a lasing transition driven by fermionic population inversion.

The total carrier density per quantum well (QW) at threshold is estimated to be $n_{th} \sim 4 \times 10^{11} \text{ cm}^{-2} > n_{Mott}$ (see Methods for details), consistent with the onset of population inversion and fermionic gain. We note that density estimates in polariton systems typically carry large uncertainties; therefore they should be used not for identification of the many-body phases but rather as a consistency check. In our experiment, regardless of the exact value of the density, the carrier reservoir that screens the electron-hole interaction in the TM exciton also screens the electron-hole interaction in the TE polariton; hence the direct observation of the Mott transition in TM confirms the fermionic nature of the gain medium.

To analyze the microscopic picture underlying the experimental observation, we develop a theory based on a non-equilibrium Green's function approach to treat self-consistently the entire fermionic system as an open dissipative and pumped system. The theory needs to correctly predict both the frequency shift due to density-dependent Coulomb interaction effects and the onset of

fermionic gain even at the presence of Coulomb interactions. The latter requires the ability to avoid artifacts in the gain spectra²⁷, which we achieve by including electronic correlations due to screening and the resulting partial cancellation of self-energy and e-h vertex contributions (c.f. Ref. ²⁸). Early theories that laid the foundation of the concept of polariton BCS states used localized 2-level states represented as fermions to model the electronic system ¹¹. Later work considered a realistic electronic band structure and 2-dimensional Coulomb interaction in the Hartree-Fock approximation ^{12,13}, but was limited to a closed, quasi-equilibrium, T=0K polariton system, which we call an “ideal polariton BCS state”. A more recent work considered an open, dissipative and pumped system, but utilized a contact potential rather than a 2-dimensional Coulomb potential ²⁹. Since BCS states are characterized by strong correlations among electrons and holes widely distributed in the configuration space, we use in our theory the 2-dimensional Coulomb potential and electronic correlations and thereby extend the description of the electronic system in^{12,13,29} beyond the Hartree-Fock approximation. We also treat the two linear polarization components (TE and TM) fully self-consistently. The incoherent pump is parameterized by the pump density n_p . Full details of the theory are given in the Supplementary Information.

Fig. 3c shows a representative result, with parameters chosen to correspond to the experiment (cavity-exciton detuning 1 meV, cavity decay rate 0.2 meV, exciton binding energy 12 meV, normal-mode splitting 12 meV). We use a pump-dependent effective electron temperature to account for pump-induced heating, $T[\text{K}] = 40 + 50n_p a_B^2$ (T models the dynamic equilibrium between high-energy pump and e-h pair recombination). The results are rather insensitive to the exact input parameters; qualitatively similar results for fixed temperature are shown in the Supplementary

Information.

The results reproduce all observed experimental features with excellent quantitative agreement. For the TM exciton, we obtain a blue-shift accompanied by strong band gap renormalization. At $n_p \sim 0.1n_{Mott}$, the exciton merges with the renormalized band gap and dissociates, which corresponds well to the observed disappearance of the exciton resonance into band-edge absorption. Further increasing density, we obtain gain due to population inversion, in agreement with the measured gain in TM field.

Gain in the TM field implies directly gain in the TE field. This is because the equations for the TE and TM interband polarization differ only in that they contain different light field amplitudes. The Coulomb interaction terms as well as the distribution functions that enter the equations, for example as the inversion or Pauli blocking factor, are the same. Therefore, TE lasing is expected as the polariton resonance enters the gain region, as is observed experimentally (Fig. 3b).

The Mott transition and fermionic gain reproduced by the theory confirm that the observed lasing transition is not an exciton-polariton BEC. At the same time, Coulomb effects continue to play a substantial role in the laser, rendering characteristics distinct from the photon laser but similar to the ideal polariton BCS state. A first manifestation is the spectral shift of the lasing state. As shown in Fig. 3c and in agreement with experimental results, the TE mode frequency shows a continuous blue-shift across the threshold, remaining significantly below that of the photon laser but tracking closely the ideal BCS state. In comparison, with Coulomb interactions turned off, we obtain photon lasing near the cavity frequency similar to the observed photon lasing in device II.

With the theory reproducing quantitatively the spectral properties measured in the experiment, we furthermore use the theory to examine the reciprocal-space carrier distribution functions $f(k)$ and the electron-hole interband polarization $|P(k)|$, which characterize the microscopic mechanism of the lasing transition. As shown in Fig. 4, both $f(k)$ and $|P(k)|$ of the polariton laser are qualitatively similar to those of an ideal BCS state but different from those of a photon laser.

As seen in Fig. 4a, $f(k)$ of both the ideal BCS state and the polariton laser saturate at values close to 0.5, while $f(k)$ of the photon laser approaches unity above threshold. Sharp kinetic holes can develop in the distribution functions of the photon laser, shown here with a small dephasing of 0.15 meV for clarity, but not in the polariton laser or the ideal BCS state. These results for the polariton laser and the BCS state are largely insensitive to the value of the dephasing.

More revealing is the interband polarizations $|P(k)|$, corresponding to the order parameter (Fig. 4b). For a photon laser, it is sharply peaked below and zero at the transparency wave vector, which corresponds to the quasi-chemical potential. In contrast, $|P(k)|$ of both the BCS polariton laser and the ideal BCS state (cf. ¹³) do not vanish at the transparency wave vector and are instead broadly distributed in the reciprocal space, indicating bound states even at densities n where the mean distance between polaritons becomes comparable to the Bohr radius a_B , i.e. $na_B^2 \approx 1$. The magnitude of $|P(k)|$ in our polariton laser is smaller than that of the ideal BCS due to cavity dissipation and dephasing.

Lastly, we estimate the BCS gap corresponding to the minimum pair-breaking excitation energy $2 \min_k E^{xc}(\mathbf{k})$. The phenomenological estimate uses the same formal expression of the

excitation energies of electrons and hole in BEC/BCS state $E^{xc}(\mathbf{k})$ and a minimization with respect to \mathbf{k} . As shown in Fig. 4c, the pair gap opens at a density corresponding to the BCS regime (see Fig 3c and increases to about 7 meV at twice threshold. From Fig. 4c we see that the gap is substantially smaller than that in the ideal system, which is expected due to cavity dissipation and dephasing and is consistent with the reduced order parameter $|P(k)|$. Such a reduction of the gap due to losses was predicted in Ref. ³⁰. Further discussion and results for the dependence of our phenomenological gap estimate on the dephasing rate are given in the Supplementary Information.

Our present experiment is not sensitive to non-lasing states within the stop band of the cavity and hence cannot measure the gap. Experiments to directly probe the BCS gap may include intra-band terahertz spectroscopy³¹. We caution that an experimental observation of a gap in the excitation spectrum is by itself insufficient to identify a BCS-like state, and theoretical analysis will be needed to distinguish between a BCS gap and spectral hole burning in a photon laser.

In conclusion, we demonstrate a BCS-like polariton lasing state. We summarize our results in Fig. 1e, where we highlight in green (blue) the properties we used to distinguish our BCS-like polariton laser from a polariton BEC (photon laser). The BCS-like polariton is different from a photon laser by the preservation of a bound state, in the form of an e-h-polariton, manifested in spectral features including an emission linewidth that remains narrow and emission frequency well below the cavity or exciton resonance frequencies without sudden shifts. These spectral features are distinct from a photon laser but closely resemble a polariton BEC. However, we unambiguously distinguish our system from a BEC-like state by measurement of the absorption spectra of

the electronic reservoir, showing our polariton laser is formed above the Mott density where excitons no longer exist, and the gain is provided by inverted electronic bands. The experimental observations are described quantitatively by a fermionic theory that extends the ideal BCS theory to an open, pumped and dissipative system at non-zero temperature. The theory, validated by the experiments, furthermore confirms the microscopic origin of the BCS state by revealing the crucial role of electron-hole interactions for the formation of the BCS state and showing electron distributions and interband coherences that are qualitatively similar to the zero-temperature polariton BCS states. A pair-breaking excitation gap opens in the BCS-like state, but is substantially reduced from that of an ideal polariton BCS state due to the elevated electron temperature, dephasing and cavity dissipation. Future work may probe the gap using intraband terahertz spectroscopy, observe the smooth crossovers among the BEC, BCS and photon lasing states, and explore conditions to realize other possible phases of the electron–hole–photon coupled system.

Methods

Microcavity sample The samples have three sets of four 12 nm-wide GaAs quantum wells with 4 nm AlAs barriers embedded at the three central antinodes of a $\lambda/2$ AlAs cavity. The bottom-mirror is a distributed Bragg reflector (DBR) with 30 pairs of $\text{Al}_{0.15}\text{Ga}_{0.85}\text{As}/\text{AlAs}$ layers. The top-mirror consists of 2.5 pairs of DBR and an $\text{Al}_{0.15}\text{Ga}_{0.85}\text{As}$ sub-wavelength grating suspending over the DBR. The grating is about 80 nm thick, with a 40% duty cycle and a grating period of 520 nm. The lower polariton (LP) and upper polariton (UP) resonances of each device are measured by reflection and low-power photoluminescence spectroscopy (see examples in Supple-

mental Information Fig. S7 and Fig. 2a). The exciton resonances are measured from the unetched part next to the device (see examples in Supplemental Information Fig. S3). Using the measured LP, UP and exciton resonances, we estimate the cavity resonance frequency, detuning, and normal mode splitting for each grating device. The size of the gratings is $7.5 \mu\text{m} \times 7.5 \mu\text{m}$. The different reflectance under the grating and outside the grating leads to laterally-confined, fully discrete TE-cavity and TE-polariton modes as evident from Fig. 2a. The sample is kept at 10 K in Janis ST-500 or Montana CR-509 cryostat for all the measurements.

Time-resolved two-color pump-probe measurement The sample is excited at 784 nm, about 30 meV above the exciton resonance, with a continuous wave (cw) laser focused to a Gaussian spot of about $3 \mu\text{m}$ in diameter at the center of the square grating. We use a TM-polarized pump to achieve higher absorption efficiency since this wavelength is still inside the stop-band of the grating for the TE polarization.

A TM-polarized resonant pulsed laser of less than 150 fs pulsewidth is used as a probe and is spatially overlapping with the pump. To measure the PL without the probe, spectrally resolved real-space and Fourier space images of the emission are collected via a 4f confocal relay into a spectrometer. For absorption measurements, both the reflected probe and the emission from the cavity system are sent to a streak camera after going through a monochromator. The reflected probe appears as a resolution-limited sharp peak in time in the streak image whereas the PL is cw and has uniform intensity in time. Hence, the PL is readily subtracted from the reflection. We integrate over the whole pulse to obtain the total intensity of reflected pulse, which is then divided by the reflection spectra from a reference gold mirror to produce the reflection spectra of the microcavity

system.

Measuring the bandwidth of the optical gain To determine the gain bandwidth requires measurement of the absolute reflectivity, which we obtain by a two-step calibration process. We first calibrate the reflectivity by normalizing the reflected pulse laser intensity on the sample to that on a gold mirror mounted in the cryostat next to the sample. There is still error due to imperfect reflection from the gold mirror as well as laser fluctuation and slight changes in the optical path when moving between the sample and the mirror. We then estimate and correct for the error using a spectral regime well below any cavity resonances but still inside the DBR stop band, where the reflectivity should be unity at no or low pump powers. As shown in Fig. 3a, such a spectra region corresponds to 1.53 – 1.54 eV, where the reflectivity is close to 1 and vary within about 2.4%. Hence we use the mean of the reflectivity in this spectral region between 0 μW to 500 μW pump power as a reference of unity. This allows us to accurately determine deviation from unity in the reflection spectra.

Gain is identified where a local maximum of the reflectivity between 1.54 – 1.55 eV is above unity as determined from above. The uncertainty of the gain boundary is estimated by dividing the standard deviation σ of the reference reflectivity by the local slope at the boundary.

Estimating the carrier density in the experiments We estimate an experimental pump density, corresponding to the pump density n_p in the theory, based on the absorption of the pump laser and

the photoluminescence (PL) decay time of the TM polarized emission:

$$\Phi_{pump} = P \frac{\lambda}{hc} \eta \alpha, \quad (1)$$

$$n_{pump} = \Phi_{pump} \tau \frac{1}{A} \frac{1}{N_{QW}}. \quad (2)$$

Here Φ_{pump} is the population of carriers excited by the pump in unit time. P is the pump laser power measured before the objective lens. $\eta = 0.7$ is the transmission of the objective lens; α is the total absorption of the pump; hc/λ is the photon energy at the excitation wavelength; τ is the average lifetime of carriers. A is the diffusion area of the carriers measured from real-space PL (example and pump power dependence given in Section. II), and N_{QW} is the number of QWs in the cavity. To determine α , we measure independently the reflectivity of a TM-polarized laser at the excitation wavelength of 784 nm. At this wavelength, the top mirror has low reflectivity; the bottom mirror has very high reflectivity and there is negligible transmission through the bottom mirror and therefore negligible absorption in the substrate. The materials of the DBR and grating layers also have larger band gap than the QWs and their absorption should be very small and is ignored. We assume the pump laser is either reflected, or absorbed by the QWs, and obtain $\alpha = 1 - R$. α and A vary among different devices. For the device shown in Fig. 3 of the main text, $\alpha \sim 0.3$ and $A \sim 32 \mu\text{m}^2$. We determine τ from the decay time of TM emission, measured by time-resolved PL of the TM emission with a pulsed excitation laser centered at the same wavelength as the cw pump laser used in the main measurement. It is found to be around 600 ps with the excitation power ranging from 1 μW to 300 μW . Non-radiative processes are ignored.

Below threshold, in the linear regime, the steady-state carrier density $n_{carrier}$ is equal to

the pump density n_{pump} . Above threshold, it is necessary to account for the strong, superlinear emission from the lasing mode. We assume that all decay processes other than the laser emission are still linear and proportional to the carrier density. Therefore, we subtract the emission rate of the laser Φ_{laser} from the pump to get an estimate of the carrier density:

$$\Phi_{laser} = N_c \frac{1}{\eta_{col}} \frac{A_{k_{mode}}}{A_{k_{col}}},$$

$$n_{carrier} = (\Phi_{pump} - \Phi_{laser}) \tau \frac{1}{A} \frac{1}{N_{QW}}.$$

Here N_c is the collected photon count from the emission of the lasing mode, $\eta_{col} = 2.85 \times 10^{-3}$ is the independently calibrated total efficiency, and $A_{k_{mode}}/A_{k_{col}} \sim 7.5$ is the ratio of the area of the lasing mode to the area of collection in Fourier space, which also varies among devices.

In this density estimation, quantities P , λ , N_{QW} , η , η_{col} , R , τ , and N_c are directly measured. α is estimated from R . A , $A_{k_{mode}}$, $A_{k_{col}}$ are estimated based on measured 1d spatial profiles of the emission along x and y directions. This estimation aims to provide an upper bound of density but should be within small uncertainty.

1. Fraser, M. D., Höfling, S. & Yamamoto, Y. Physics and applications of exciton-polariton lasers. *Nature Materials* **15**, 1049–1052 (2016).
2. Sanvitto, D. & Kna-Cohen, S. The road towards polaritonic devices. *Nature Materials* **15**, 1061–1073 (2016).
3. Deng, H., Haug, H. & Yamamoto, Y. Exciton-polariton Bose-Einstein condensation. *Reviews of Modern Physics* **82**, 1489 (2010).

4. Keeling, J., Marchetti, F. M., Szymańska, M. H. & Littlewood, P. B. Collective coherence in planar semiconductor microcavities. *Semiconductor Science and Technology* **22**, R1–R26 (2007).
5. Dalfovo, F., Giorgini, S., Pitaevskii, L. P. & Stringari, S. Theory of Bose-Einstein condensation in trapped gases. *Reviews of Modern Physics* **71**, 463 (1999).
6. Leggett, A. J. Bose-Einstein condensation in the alkali gases: Some fundamental concepts. *Reviews of Modern Physics* **73**, 307 (2001).
7. Bardeen, J., Cooper, L. N. & Schrieffer, J. R. Theory of Superconductivity. *Physical Review* **108**, 1175–1204 (1957).
8. Chow, W. W., Koch, S. W. & Sargent, M. *Semiconductor-Laser Physics* (Springer, Berlin, Heidelberg, Berlin, Heidelberg, 1994).
9. Carusotto, I. & Ciuti, C. Quantum fluids of light. *Reviews of Modern Physics* **85**, 299–366 (2013).
10. Imamoglu, A. & Ram, R. J. Quantum dynamics of exciton lasers. *Phys. Lett. A* **214**, 193 (1996).
11. Keeling, J., Eastham, P. R., Szymanska, M. H. & Littlewood, P. B. BCS-BEC crossover in a system of microcavity polaritons. *Physical Review B* **72**, 115320 (2005).
12. Kamide, K. & Ogawa, T. What Determines the Wave Function of Electron-Hole Pairs in Polariton Condensates? *Physical Review Letters* **105**, 056401 (2010).

13. Byrnes, T., Horikiri, T., Ishida, N. & Yamamoto, Y. BCS Wave-Function Approach to the BEC-BCS Crossover of Exciton-Polariton Condensates. *Physical Review Letters* **105**, 186402 (2010).
14. Szymanska, M. H., Littlewood, P. B. & Simons, B. D. Polariton condensation and lasing in optical microcavities: The decoherence-driven crossover. *Phys. Rev. A* **68**, 013818 (2003).
15. Keldysh, L. & Kozlov, Y. Collective properties of excitons in semiconductors. *Sov. Phys. JETP* **27**, 521–528 (1968).
16. Comte, C. & Nozieres, P. Exciton Bose condensation: the ground state of an electron-hole gas i. mean field description of a simplified model. *J. Physique* **43**, 1069–1081 (1982).
17. Littlewood, P. B. *et al.* Models of coherent exciton condensation. *Journal of Physics: Condensed Matter* **16**, S3597–S3620 (2004).
18. Kremp, D., Semkat, D. & Henneberger, K. Quantum condensation in electron-hole plasmas. *Phys. Rev. B* **78**, 125315 (2008).
19. Deng, H., Weihs, G., Santori, C., Bloch, J. & Yamamoto, Y. Condensation of Semiconductor Microcavity Exciton Polaritons. *Science* **298**, 199–202 (2002).
20. Bajoni, D. *et al.* Polariton laser using single micropillar GaAs-GaAlAs semiconductor cavities. *Physical Review Letters* **100**, 047401 (2008).
21. Kim, S. *et al.* Coherent Polariton Laser. *Phys. Rev. X* **6**, 011026 (2016).

22. Zhang, B. *et al.* Zero-dimensional polariton laser in a subwavelength grating-based vertical microcavity. *Light: Science & Applications* **3**, e135 (2014).
23. Kasprzak, J. *et al.* Bose–Einstein condensation of exciton polaritons. *Nature* **443**, 409–414 (2006).
24. Balili, R., Hartwell, V., Snoke, D., Pfeiffer, L. & West, K. Bose-Einstein Condensation of Microcavity Polaritons in a Trap. *Science* **316**, 1007–1010 (2007).
25. Bajoni, D., Senellart, P., Lemaître, A. & Bloch, J. Photon lasing in GaAs microcavity: Similarities with a polariton condensate. *Physical Review B* **76**, 201305R (2007).
26. Balili, R., Nelsen, B., Snoke, D. W., Pfeiffer, L. & West, K. Role of the stress trap in the polariton quasiequilibrium condensation in GaAs microcavities. *Physical Review B* **79**, 075319 (2009).
27. Girndt, A. *et al.* Multi-band bloch equations and gain spectra of highly excited ii-vi semiconductor quantum wells. *Phys. Stat. Sol (b)* **202**, 725 – 739 (1997).
28. Semkat, D. *et al.* Ionization equilibrium in an excited semiconductor: Mott transition versus Bose-Einstein condensation. *Phys. Rev. B* **80**, 155201 (2009).
29. Yamaguchi, M., Kamide, K., Nii, R., Ogawa, T. & Yamamoto, Y. Second Thresholds in BEC-BCS-Laser Crossover of Exciton-Polariton Systems. *Physical Review Letters* **111**, 026404 (2013).

30. Szymanska, M., Littlewood, P. & Simons, B. Polariton condensation and lasing in optical microcavities: The decoherence-driven crossover. *Phys. Rev. A* **68**, 013818 (2003).
31. Ménard, J.-M. *et al.* Revealing the dark side of a bright excitonpolariton condensate. *Nature Communications* **5**, 4648 (2014).

Acknowledgements J.H, Z.W. and H.D. acknowledge financial support from the US Air Force Office of Scientific Research under grant FA9550-15-1-0240 and the US NSF under grant DMR 1150593. The Würzburg group gratefully acknowledges support by the state of Bavaria. N. H. K. and R. B acknowledge financial support from the US NSF under grant ECCS-1406673 and CPU time at the University of Arizona HPC Center.

Author contributions J.H. and Z.W. performed the experiments and data analysis. Z.W. and H.D. designed the experiments. S.K. fabricated the devices on the wafer. S.B., C.S. and S.H. grew the wafer. N.H.K. and R.B. performed the theoretical analysis and simulations. J.H. H.D. and R.B. wrote the manuscript. H.D. and R.B. supervised the project. All authors discussed the results and the manuscript.

Competing interests The authors declare that they have no competing financial interests.

Materials & Correspondence Data available on request from the authors. Code for the theoretical calculations available on request from the authors. Correspondence and requests for materials should be addressed to H.D. (email: dengh@umich.edu) and R.B. (email: binder@optics.arizona.edu).

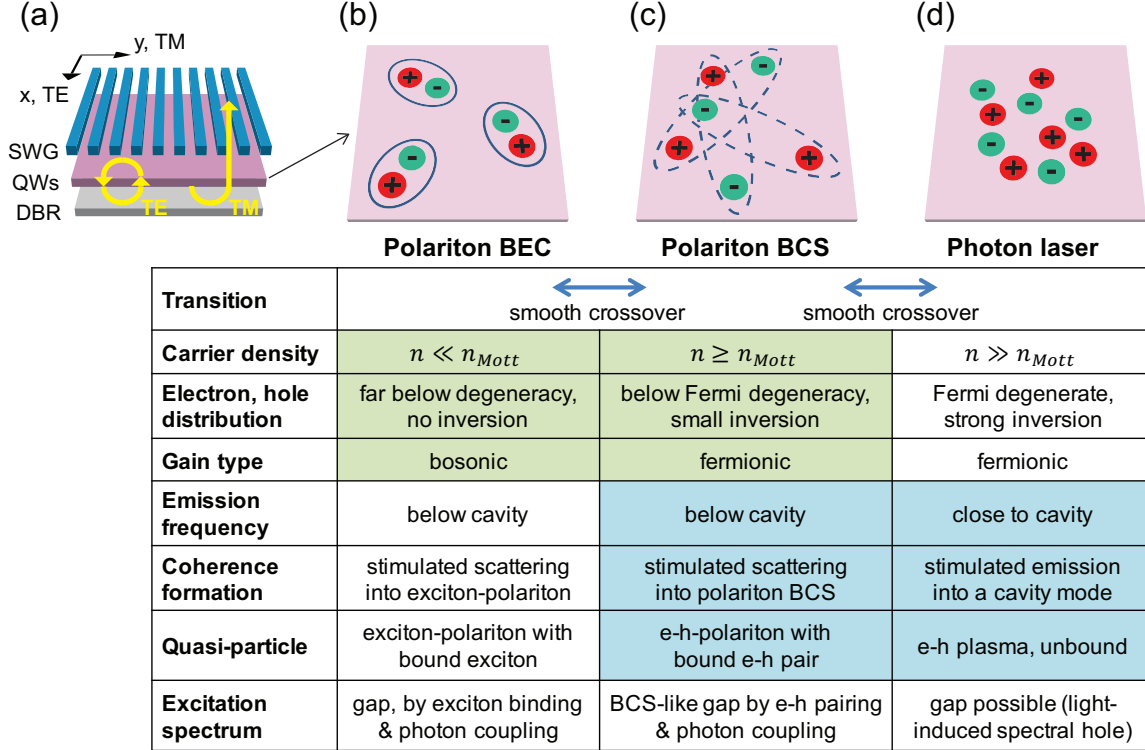


Figure 1: **Comparison of the polariton BEC, polariton BCS and photon laser.** (a) A schematic of the sub-wavelength grating (SWG) based microcavity that allows access to the electronic reservoir of a polariton system. Quantum wells (QWs) are embedded in the cavity formed by an SWG and a distributed Bragg reflector (DBR). Fields polarized parallel to the bars (TE) are well confined in the cavity while the perpendicularly polarized fields (TM) transmit through the SWG. (b-d) Illustrations of three possible many-body states in the system with different quasi-particles in the electronic medium: (b) polariton BEC with boson-like excitons (bound electron-hole, e-h, pairs at low density), (c) polariton BCS (bound e-h pairs at elevated density), and (d) a conventional photon laser with plasmas of unbound e-h pairs. Polaritons are formed in (b) and (c) via strong photon coupling. The table summarizes key properties of the three many-body states. The properties confirmed for our system are highlighted through colors with green and blue table cells showing properties that distinguish our polariton BCS-like laser from a polariton BEC and photon laser, respectively.

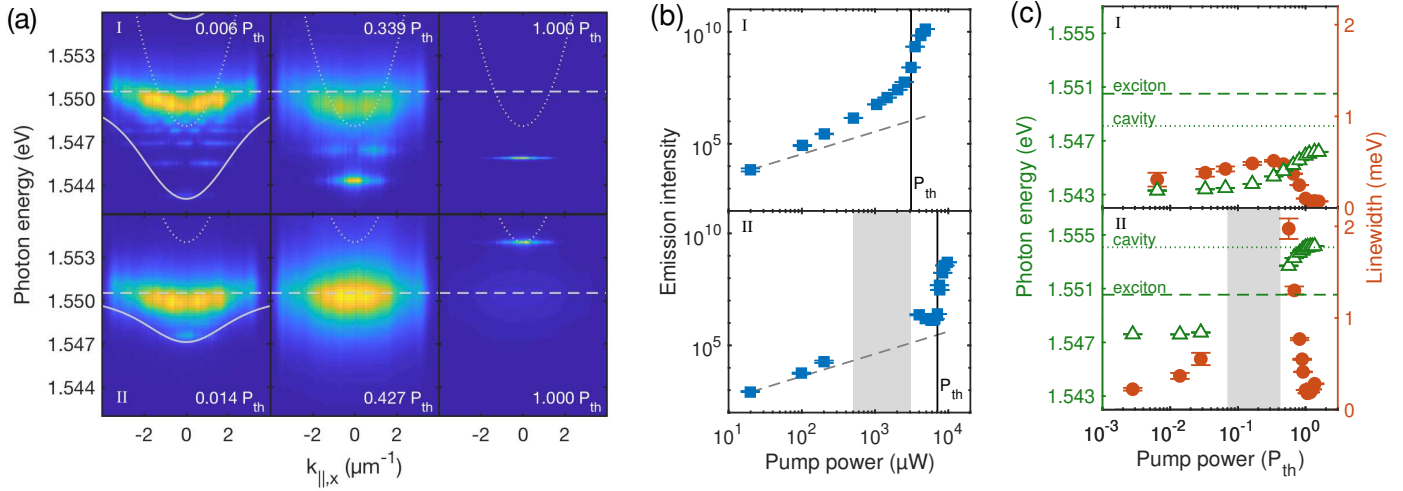


Figure 2: **Emission properties of a BCS-like polariton laser (device I, top row) and a photon laser (device II, bottom row).** (a) Fourier-space spectral images of TE-polarized emission from below to above the lasing threshold at $k_{||,y} \sim 0$ at pump powers as labeled. The middle panels correspond to, respectively, where the $k_{||} = 0$ mode has the largest linewidth in device I (top) and shifts/disappears into the TM background in device II (bottom). The dashed lines mark the exciton resonances measured outside the grating region by reflection without a pump. The dotted/solid curves are the calculated empty cavity/polariton dispersions assuming no in-plane confinement; they are based on the measured exciton energy and the lower and upper polariton energies measured from TE reflection without pump (see Supplementary information). The detunings are -2.4 meV and +3.5 meV respectively for device I and II. (b) The emission intensity of the TE $k_{||} = 0$ mode vs. the pump power. The dashed line is a reference of linear dependence. (c) Pump power dependence of the emission photon energy (open green squares) and linewidth (filled orange circles) of the TE $k_{||} = 0$ modes. The empty cavity at $k_{||} = 0$ (dotted lines) and exciton (dashed lines) resonances are also shown. In (b) and (c), the grey region corresponds to where the TE ground state disappears into a broad background at the exciton energy; the vertical solid lines mark the lasing threshold.

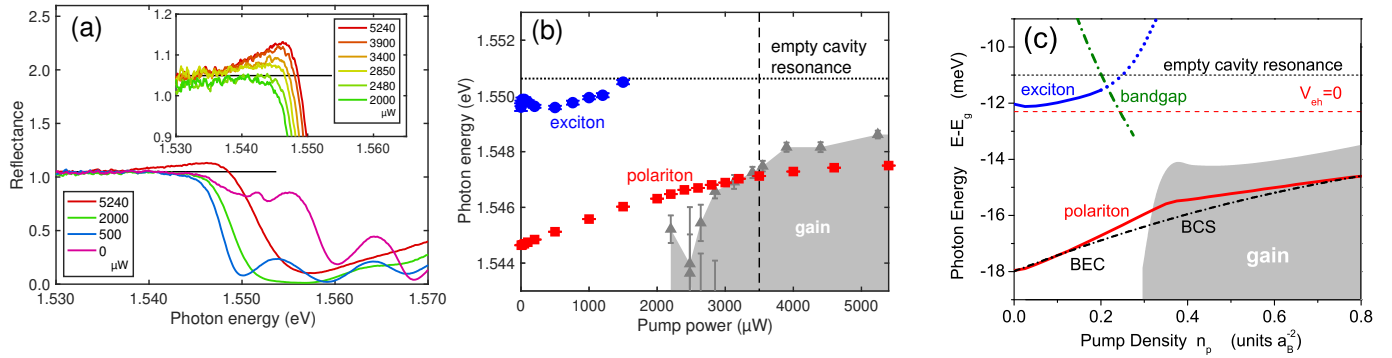


Figure 3: Measured and calculated gain and energetic positions of a BCS-like polariton laser.

(a) TM reflection spectra for a BCS-like polariton laser at different pump power. The horizontal black lines mark reflectivity of 1 (see Methods for calibration of the reflectivity). Inset: zoom-in near the gain.

(b) Measured pump power dependence of the energetic positions of the TE $k_{\parallel} = 0$ mode (red squares), TM exciton (solid blue circles) and the spectral bounds of gain (grey triangles). Error bars on the bounds are obtained by dividing the standard deviation of the reference of unity reflectivity by the local slope at the boundary. The empty cavity resonance is marked by the black dotted line. The BCS polariton lasing threshold, marked by the black dashed line, coincides with the onset of the fermionic gain. The exciton mode, extracted from TM reflection spectra (examples in the Supplementary Information), is no longer resolvable above $1500 \mu\text{W}$, due to dissociation of the excitons above the Mott transition.

(c) Calculated pump density (n_p) dependence of the energetic positions of the TE ground state (red), TM exciton (blue solid line), gain region (grey area), ideal polariton BEC/BCS quasi-chemical potential assuming density $n = n_p$ (dash-dotted line), the TE emission without e-h interaction corresponding to an ideal photon laser, renormalized bandgap (green dash-dotted line), and empty cavity resonance (black dotted line). $a_B = 14 \text{ nm}$ and $E_g = 1.562 \text{ eV}$ are the exciton Bohr radius and quantum well bandgap energy, respectively.

Effective electron temperature $T[K] = 40 + 50 n_p a_B^2$.

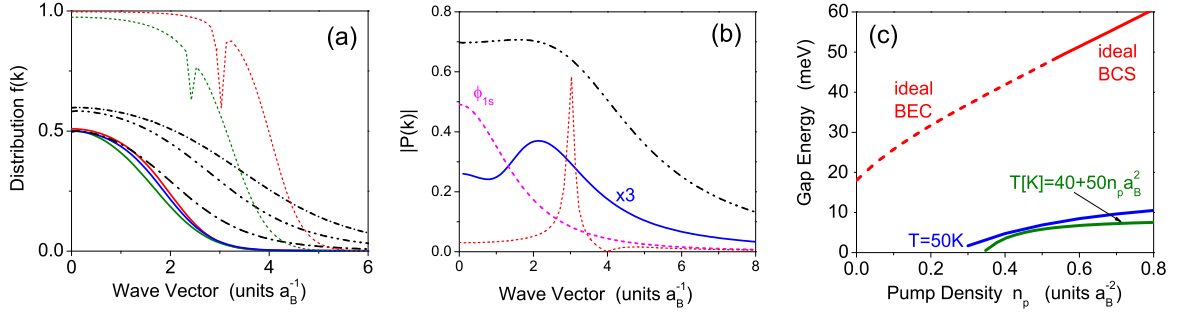


Figure 4: **Carrier distributions and wave functions.** (a) Distribution functions at $T = 50\text{K}$. Solid lines: full calculation at pump densities $n_p a_B^2 = 0.3, 0.45$ and 0.6 (threshold pump density $n_p^{th} \approx 0.3 a_B^{-2}$), $\gamma = 1.5\text{meV}$. Short dashed lines: without e-h interaction at $n_p a_B^2 = 1.6$ (green) and 2.6 (red), $n_p^{th} \approx 1 a_B^{-2}$, $\gamma = 0.15\text{ meV}$. Black lines: ideal polariton BCS at densities $n a_B^2 = 0.6$ (long dash-dot), 1.2 (dash-dot-dot) and 1.8 (short dash-dot), showing that at large densities $f_{BCS}(k=0)$ saturates at about 0.6 . (b) Corresponding magnitudes of polarizations (effective wave functions), same line styles as in (a). The dashed magenta line shows the $1s$ exciton wave function normalized to a density of $4 \times 10^{10}\text{cm}^{-2}$. (c) Pair gap energy of ideal system (red line) and phenomenological estimate of the pair gap energy of the experimental system (green and blue lines).